Modeling the Impact of Earthquake-Induced Sensitive Clay Landslide on an Exposed Pipeline Using a Large Deformation Finite Element Method

Naveel Islam
Military Institute of Science & Technology, Dhaka, Bangladesh
Kshama Roy
Northern Crescent Inc., Calgary, Alberta, Canada
Bipul Hawlader
Memorial University of Newfoundland, St. John's, NL, Canada

ABSTRACT
The sudden and mostly unpredictable landslides in sensitive clay are generally retrogressive in nature and eventually turn into a flow of failed soil mass that exerts force on the pipeline placed across the route of the flow (drag). The drag force is one of key design parameters for selection of the pipeline route. Depending upon the velocity of the debris, the drag force on the pipelines might vary with time. The large deformation finite element modeling techniques in an Eulerian framework can simulate the large deformation slope failures of sensitive clays. In the present study, the drag force on a pipeline due to the impact of the failed soil resulted from an earthquake-induced landslide is simulated. A parametric study is conducted for varying pipe size, pipe location, and soil properties.

RÉSUMÉ
Les glissements de terrain soudains et généralement imprévisibles dans l'argile sensible sont généralement de nature rétrograde et finissent par se transformer en un écoulement de masse de sol défaillant qui exerce une force sur le oleoduc placé en travers du tracé de l'écoulement (traînée). La force de traînée est l'un des paramètres clés de la conception pour de la sélection du tracé du pipeline. Selon la vitesse des débris, la force de traînée sur les oleoducs peut varier avec le temps. Les techniques de modélisation par éléments finis aux grandes déformations dans un cadre eulérien permettent de simuler les défaillances importantes des pentes de déformation des argiles sensibles. Dans la présente étude, on simule la force de traînée sur un oleoduc en raison de l'impact du sol défaillant résultant d'un glissement de terrain induit par un séisme. Une étude paramétrique est réalisée pour une taille, un emplacement et des propriétés du sol variable.

1 INTRODUCTION

Transmission pipelines are the most popular and widely used medium to transport hydrocarbons (e.g., oil and gas) over long distances. Pipelines might pass through various geological and topographic conditions and therefore, pipeline routing is a critical component for successful design and regulatory approval. Due to the environmental and safety concerns or constraints imposed by the land use, pipeline routing often requires designers to allow for crossing adverse ground (e.g., along or closer to sensitive clay slope). One of the major problems associated with pipelines is the deformation of pipelines due to movements of slope or slope failure, ground subsidence, and earthquakes (Crofts et al. 1977; Symons et al. 1982; Rumsey et al. 1982; Choo et al. 2007; Nyman et al. 2008, Wijewickreme et al. 2009; Klar and Marshall 2015). Girgin and Krausmann (2015) reported a total of 6,139 and 10,177 cases of significant pipeline incidents due to earthquake and landslides, respectively. In the Enbridge report on geohazards issues for the Northern Gateway project, Rathje (2011) showed the importance of developing a comprehensive assessment of the seismic landslide potential along the pipeline route.

A number of sensitive clay slope failure incidents have been reported in Canada. For example, the 1663 Charlevoix earthquake (magnitude M_M > 7), Québec in eastern Canada triggered large earth flows in sensitive clay that extended over a wide region of the Saguenay Fjord basin (Desjardins 1980; Filion et al. 1991; Syvitski and Schafer 1996). Many small-scale landslides in the sensitive clay, such as the Sainte-Thècle landslide in southern Québec due to the 1988 Saguenay earthquake (M_M = 5.9) (Lefebvre et al. 1992) or Notre-Dame-de-la-Salette and Mulgrave & Derry slides due to the 2010 Val des-Bois earthquake, Québec (M_M = 5.2) (Demers et al. 2014) were also reported. In general, such large- or small-scale flowslide begins with an initial rotational slide followed by a succession of rapid rotational failures under undrained conditions. During this process, part of the clayey deposit along the failure planes is transformed into a more or less liquid state that carries the overlying clay materials along the direction of the flow. Therefore, the failure extends over a large area from the initial zone of failure (Tavenas 1984; Lefebvre 1992; Demers et al. 2014).

If a pipeline crosses along or closer to sensitive clay or very soft soil slope which lies within high seismic areas, then the pipeline might experience an earthquake-induced sensitive clay landslide. Several pipeline failure cases due to sensitive clay slope failure have been reported in the past. For example, Schwab et al. (2004) reported the rupture of a natural gas pipeline, disrupting service to Prince Rupert for approximately 10 days, due to the sensitive glaciomarine flow slide, known as the '2003

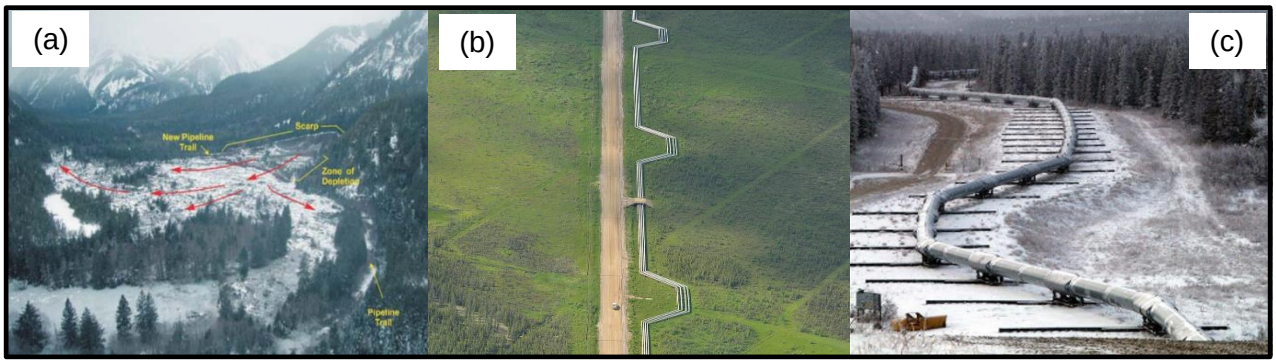

Figure 1. (a) 2003 Khyex river landslide (Schwab et al. 2004), (b) SAGD pipelines, Suncor Firebag project by Louis Helbig (2014), (c) The Trans-Alaskan pipeline by U.S. Geological Survey (2002)

Khyex river landslide' (Figure 1(a)). Any pipeline located in front of such sensitive clay slope failure will experience subsequent hits (drags) from the debris flow until unless it moves around the pipe or it can breakout of its embedment allowing the slid mass to pass beneath the pipeline system (Nyman et al. 2008).

It is a common practice to bury the pipeline; however, the cases of a section of the pipeline above the ground are not unusual. For example, most of the SAGD pipelines are aboveground (Figure 1(b)). Furthermore, pipelines might need to be laid above the ground in special environmental/design considerations; for example, some sections of the Trans-Alaska pipeline were put aboveground with special footings that allow the pipeline to move both laterally and vertically in order to maintain a seismic isolation against the rupture of a pre-existing active strike-slip fault (Figure 1(c)). In addition, natural or human activities (e.g., small slope failure, ground subsidence due to construction activities) and operating conditions (upheaval buckling) could expose the pipeline. Therefore, pipeline designers need to estimate the consequence of the impact on the aboveground pipelines caused by debris flow due to earthquake-induced sensitive clay slope failures.

Previous researchers (e.g. Dey et al. 2015; Trapper et al. 2015; Locat and Lee 2002; Masson et al. 2006) reviewed the modeling technique of sensitive clay slope failure. However, they did not show the effect of such sensitive clay slope failure on the pipelines. A number of studies investigated the drag force on suspended offshore pipeline, especially in deepwater condition (Zakeri 2009; Randolph and White 2012; Zakeri and Hawlader 2013). However, as explained in the later sections, the mechanisms of sensitive clay slope failure impact on pipeline is different from that of offshore environments.

The primary design guideline for Canadian pipelines is CSA Z662-15 Oil and Gas Pipelines Systems. Clause 4 of CSA Z662-15 deals with the design requirements for pipeline systems. However, as stated in Clause 4.2.4, the stress design requirements in the code do not include the effects of inertial earthquake loads, slope movements or earthquake-induced earth movements. The 2004 PDCR Guidelines, as well as Nyman et al. (2008), recommend that pipeline sections in landslide-prone areas need to be designed with large displacement capacity. There is currently no guideline or body of research that addresses the forces or strain transmission from a landslide to a pipeline on an inclined slope (Eichhorn and Haigh 2018).

The present study adopted the large deformation finite element modeling technique proposed by Islam et al. (2018a) for earthquake-induced sensitive clay slope failure and extends the model to study the effect of such failure on an exposed section of a pipeline located near the toe of the slope. Note that the current industry practice for geohazards analysis uses American Lifeline Alliance (ALA) guidelines to model the soil load exerted on the pipeline. However, the ALA guidelines only consider the maximum soil resistance based on the physical tests, where the pipe was moved against the soil at a constant speed. The drag force history on the pipeline resulting from an earthquake-induced sensitive clay slope failure is investigated using the following steps:

- Large deformation finite element modeling of earthquake-induced sensitive clay slope failure using the Eulerian formulation in Abaqus (Islam et al. 2018a);
- Analysis of the impact of the slope failure and debris flow on the pipeline (drag forces); and
- A parametric study for pipe diameter, pipe locations, and sensitive clay properties.

2 PROBLEM DEFINITION

A 15-m high idealized sensitive clay slope (2H:1V) with a large soil domain of 400 m length is considered in this study (Figure 2). The left and right boundaries of the model are kept at 150 m and 250 m, respectively, from the toe of the slope. A rigid pipe (Diameter, D = 300 mm, for the base case) was laid on the downslope ground surface (on the horizontal surface (ba) in Figure 2) at a distance of l (= 10 - 50 m) from the toe of the slope. Below the 30-m deep sensitive clay layer, a 15-m stiff clay layer followed by a 2-m strong base layer (high undrained Young's Modulus, E_u) is assumed (Figure 2). Saturated unit weight is used in the analysis. The earthquake excitation is applied at the bottom of the base layer as shown in Figure 2.

Figure 3 shows the input horizontal earthquake motion (acceleration vs time) used in the present study, which is applied at the base of the model (PQ in Figure 2). Note that the acceleration–time history (Figure 3) used in the present study is a modified form of the 1985 Nahanni earthquake that occurred in the Northwest Territories in Canada

(Wetmiller et al. 1988; PEER 2010). To simulate the post-quake displacement of the failed soil, the analysis is continued for a time period even after end of the earthquake until the instantaneous velocity of the soil elements becomes zero or negligible.

3 FINITE ELEMENT MODELING

The Eulerian approach available in Abaqus/Explicit Version 6.14.2 finite element (FE) software is used. The details of the FE modeling technique, including the

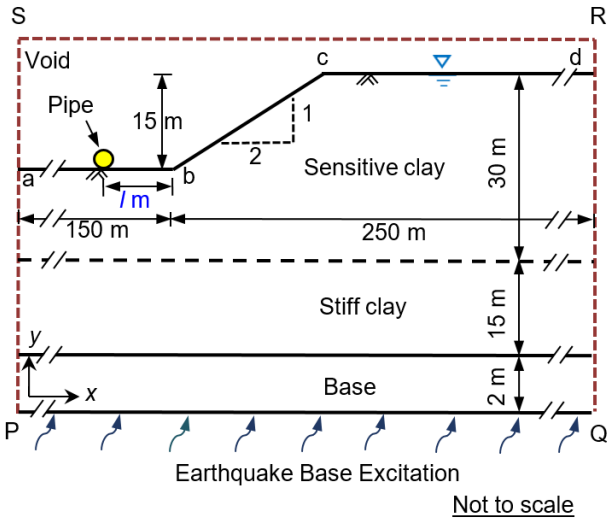

Figure 2. Geometry of the slope used in the FE modeling

earthquake-induced landslide simulations have been discussed in previous studies (Islam et al. 2018 a-b).

The soil is modeled as a Eulerian material. Since the Eulerian analysis in Abaqus allows only three-dimensional modeling, all the analyses are performed in a 3D configuration with a model of one element thickness (= 0.25 m) in the out-of-plane direction to simulate the plane strain condition. The FE domain (PQRS in Figure 2) is discretized using EC3D8R elements (8-node hexahedral linear brick, reduced integration Eulerian element with hourglass control) available in Abaqus.

The FE model in Figure 2 comprises of three parts: (1) the soil (abcdQP), (2) the pipe and (3) the void (abcdRS). The void space accommodates the displaced soil mass due to the landslide. Soil and void spaces are created in the Eulerian domain using Eulerian Volume Fraction (EVF) tool. For void space, EVF = 0 i.e. no soil parameters are defined for this abcdRS zone (Figure 2). For abcdQP zone in Figure 2, EVF is defined as unity, which indicates that the elements are filled with soil.

The objective of the present study is to obtain the drag force on a rigid pipeline fixed at a certain position. Therefore, instead of defining the pipe as a Lagrangian body together with interface conditions (e.g., smooth/rough) (Pike et al. 2014; Dutta et al. 2015; Roy et al. 2016), a cylindrical section same as the pipe is extruded from the Eulerian void. The interior surface of this section (pipe) is defined with a set of nodes where zero-velocity boundary conditions (v_x = v_y = v_z = 0) are applied and therefore, no displaced soil mass can enter inside that impermeable pipe section. The drag force (F_D) exerted by the soil on the pipe is calculated by summing the magnitude of the nodal forces along the circumference of the pipe.

To maintain the plane strain condition during the analysis, the movement of the soil perpendicular to the x-y plane is restricted by applying zero velocity boundary conditions along the z-axis. The bottom of the model (PQ) is restrained from any vertical movement and the vertical faces (SP & RQ) are restrained from any lateral movement. No boundary conditions are applied along the soil–void interface to allow the displaced soil move inside the void space. Eulerian non-reflecting boundary conditions are used on the vertical faces (SP & RQ in Figure 2). This specific boundary condition helps to avoid the reflection of incident waves during dynamic motion (Islam et al. 2018b).

The numerical analysis mainly consists of three steps: (1) gravitational loading, (2) earthquake loading, and (3) post-earthquake movement. In the first step, gravity load is applied gradually to attain geostatic stresses in the soil elements. Due to this loading, shear stresses are created in the soil elements near the slope; however, it is lower than the shear strength of the soil near the toe depth. Therefore, the slope is stable at the end of this loading step maintaining at earth pressure coefficient (K_0) equal to 1. In the second step, the earthquake motion (Figure 3) is applied horizontally at the base of the model, PQ (Figure 2). Finally, after the completion of the earthquake loading step, the analysis is continued until the instantaneous velocity of the soil elements becomes almost negligible.

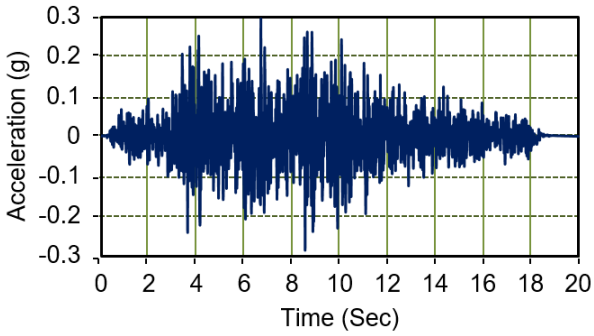

Figure 3. Acceleration–time history used in FE analysis

4 CONSTITUTIVE MODELING OF SOIL

The mobilized undrained shear strength (s_u) of sensitive clay is modeled as a function of accumulated plastic shear strain as shown in Figure 4. The soil is modeled as elastic–plastic material, by defining the von Mises yield strength (= $2s_u$), considering a total stress analysis. Before the peak s_u, the stress–strain behaviour is linear elastic. The initial peak s_{u0} remains constant up to δ_{pc}. The s_u drops quickly after $\delta_{pc.}$ A linear degradation of s_u with accumulated shear strains for cyclic loading was suggested in previous studies (e.g. Nadim 1998, Pestana and Nadim 2000). However,

Dey et al. (2015) suggested the following exponential relationship (Eq. 1) of shear strength mobilization for

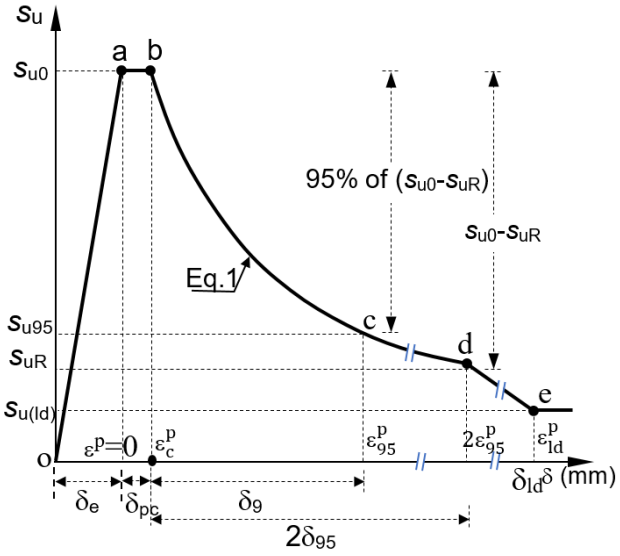

Figure 4. Stress-displacement behavior used in FE modeling (Dey et al. 2015)

sensitive clay (bcd in Figure 4)

$$s_{uR} = s_{uR} + (s_{u0} - s_{uR})\, e^{-3\delta/\delta_{95}} \text{ ; for } 0 \le \delta \le 2\delta_{95} \qquad [1]$$

Where, s_{uR} is the values of s_u at large δ and δ_{95} is the value of δ at which the undrained shear strength of the soil is reduced by 95% of (s_{u0}-s_{uR}). Equation [1] is a modified form of shear strength mobilization equation proposed by Einav and Randolph (2005). After s_{uR} (point d in Figure 4), the mobilized s_u reduces slowly with shear displacement. The reduction of s_u in this zone is defined by a linear line de, which shows that the shear strength reduces to a small value $s_{u(ld)}$ at large displacement δ_{ld}. After δ_{ld}, $s_{u(ld)}$ remains constant.

Table 1 shows the geotechnical parameters used in the present FE analyses unless otherwise mentioned. Estimation of the parameters was made from laboratory tests, interpretation of test data and numerical studies of landslides in sensitive clays from the literature (e.g. Tavenas et al. 1983; Stark and Contreras 1998; Leroueil, 2001). The variations of s_u with depth (initial condition) and accumulated plastic shear strain (during failure) are defined in Abaqus using a user-defined subroutine in VUSDFLD. The subroutine code ensures that the displaced soil during failure carries the initial value of s_{u0}. The selection and validation of the parameters can be found at Islam et al. (2018 a-b).

5 RESULTS

During the failure of the slope, the equivalent plastic shear strains ϵ_q^p (= PEEQVAVG in Abaqus) concentrates in narrow shear bands due to the mobilization of s_u in the failed soil mass. The ϵ_q^p is related to the engineering plastic shear strain (γ_p) as $\epsilon_q^p = \gamma_p / \sqrt{3}$, where, $\gamma_p = \delta / t_{FE}$ for simple shear conditions and t_{FE} is the length of the cubical elements used in this study. The zones of very high ϵ_q^p indicate the failure surfaces when the soil block displaces at larger distances from the initial condition.

Table 1. Geotechnical Parameters

Parameters	Value		
	Sensitive Clay	Stiff Clay	Base
Undrained Young's Modulus, E_u (MPa)	10	10	100
Undrained Poisson's ratio, v_u	0.495		
Peak undrained shear strength, s_{u0} (kPa)	Linear§		
Remoulded undrained shear strength, s_{uR} (kPa)	s_{u0}/3.5	s_{u0}	—
Large displacement undrained shear strength, s_{uld} (kPa)	s_{u0}/16	s_{u0}	—
Plastic shear displacement for initiation of softening, δ_{pc} (m)*	0.006	—	
Plastic shear displacement for 95% degradation of soil strength, δ_{95} (m)	0.035	—	—
Plastic shear displacement for large displacement undrained shear strength, δ_{ld} (m)	2	—	—
Saturated unit weight of soil, γ_{sat} (kN/m^3)	20		
Rayleigh damping parameter, β	0.000375		-

§ s_{u0} varies linearly with depth below the crest of the slope (z) as s_{u0} (in kPa) = 25+2z (in m)
* for FE input, the plastic shear strain is calculated using δ and thickness of the element

5.1 Propagation of shear bands

Figure 5 shows the formation and propagation of shear bands during the earthquake and post-earthquake stages for the slope defined in Figure 2 with D = 300 mm, l = 10 m. Note that the pipe shown in Figure 5 has been enlarged for better presentation. A rotational slide initiates in the slope at t =8.5s of the earthquake (Figure 5(a)). With further movement of the failed soil mass out of the crater, a shallower slide starts to generate at the back of the slope that retrogrates backward horizontally forming additional failure of soil blocks (Figure 5(b)-(c)). The broken line in Figure 5 shows the initial layout of the slope. During this time period (t = 8.5 -13.7s), the displaced soil blocks at larger distances are generally broken into pieces by the generation of additional shear bands within the failed blocks. Due to the progressive shear band formation, two types of soil elements, intact (soil elements between the shear bands where significant shear strain has not been generated) and failed (where high shear strain has been generated), can be seen in Figure 5(b – f). Note that both the intact and failed soil blocks might hit the pipe with time.

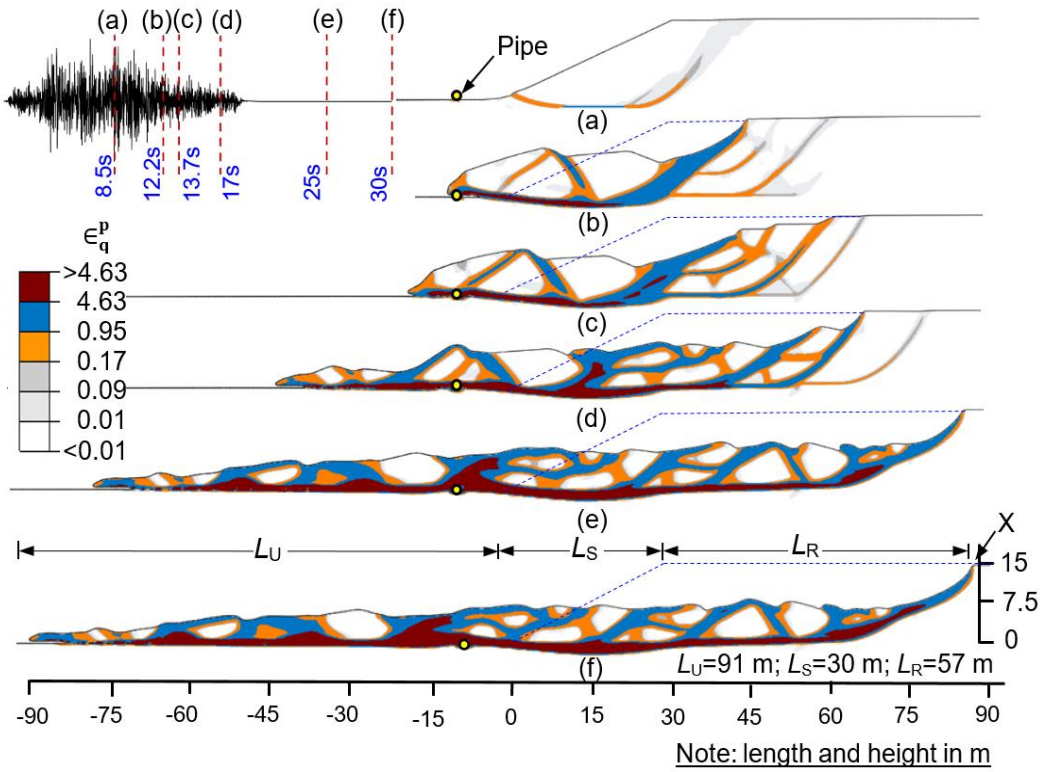

Figure 5. Formation of failure planes during the landslide

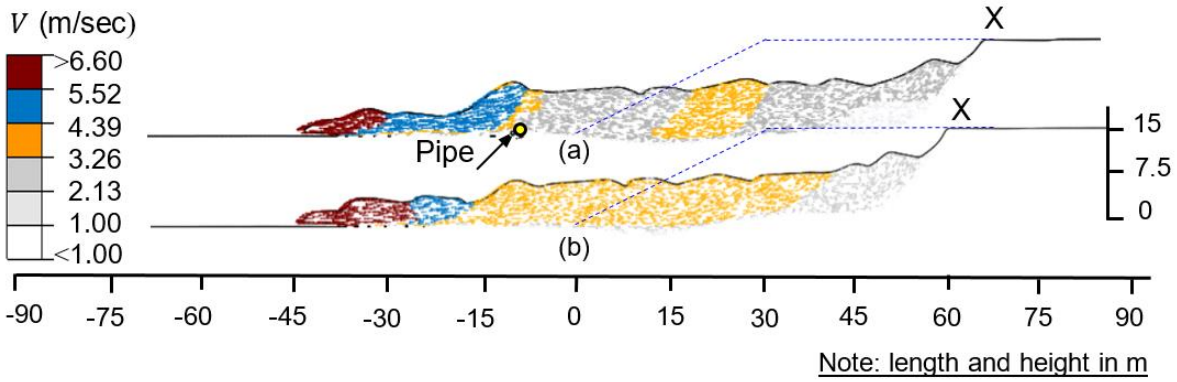

Figure 6. Velocity vector with (a) pipe and (b) without pipe at 17 secs of earthquake

During the post-earthquake stage (Figure 5(e) - (f)), the debris continues to runout from the crater, reduces the soil supports and hence forms a backscarp on the right side of the slope until unless the velocity of the soil block completely ceases. The lateral extent of the landslide (L_E) is defined as the sum of the retrogression distance (L_R), the slope distance (L_S) and runout distance (L_U) (Figure 5(f)). Similar rotational flows were also observed in sensitive clays in Quebec due to the Val de Bois earthquake in 2010 (Demer et al. 2014) and Saguenay earthquake in 1988 (Lefebvre et al. 1992).

Figure 6(a) indicates the higher velocity of the soil debris (> 3 m/s) at the end of 17 s of earthquake stage. It also shows the distinct differences in velocity vector and debris failure pattern due to the presence of pipe, e.g. the velocity (2.13 – 3.26 m/sec) of the debris between 12 m to 15 m (Figure 6(a)) is lower when the pipe is present compared to the velocity (3.26 – 4.39 m/sec) with no pipe (Figure 6(b)). Furthermore, at this time, the distance between the toe of the slope and the rightmost backscrap point (point X in Figure 6) is larger when the pipe exists (Figure 6(a)) compared to the distance with no pipe (Figure

6(b)). Both of such lower velocity and larger distance between the toe of the slope and rightmost backstrap point are due to the fact that the pipe generally acts as an obstacle on the debris movement.

5.2 Change in Drag force with loading time

Figure 7 shows the variation of drag force (F_D) with time for D = 300 mm and l = 10 m. The soil properties used in this analysis are shown in Table 1. First 0 - 20 sec is the earthquake loading stage. F_D reaches the peak value at ~ 12 sec (point B), decreases (point C) and then increases again at ~ 15 sec (point D), decreases again (point E) and then increases at ~ 23 sec (point F). After point F, F_D decreases to point G and then increases gradually to point H. This repetitive increase and decrease in drag force is due to the combination of the velocity of the soil debris flow that hits the pipe and the location of the intact and failed (highly sheared having low s_u) soil blocks over the pipe. To explain this mechanism further, both the failure pattern (shear strain plot) and velocity profile near the pipe have been shown (Figure 8) for points B – H in Figure 7.

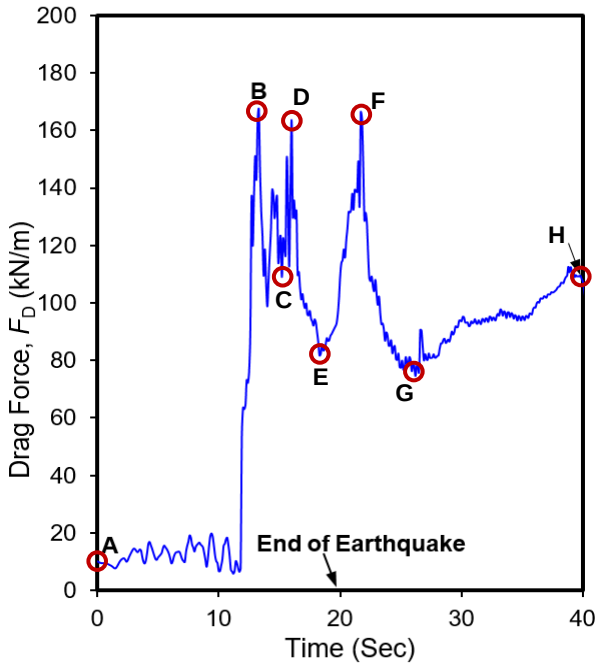

Figure 7. Drag force with loading time

As shown in Figure 8(a & h), for point B, an intact soil block exists over the pipe at this time and the velocity is high (Figure 8(h)). The shear strength of the intact soil block is higher than the failed soil block as significant plastic shear strain has been generated in the failed soil block. Therefore, the drag force is higher at point B. At point C, the velocity become lower (Figure 8(i)) and a failed soil block exists over the pipe (Figure 8(b)), which drops the drag force down. Again at point D, another intact soil block becomes evident over the pipe (Figure 8(c)) and the velocity of the debris is lower (Figure 8(j)) compared to the velocity for point B (Figure 8(h)) and hence, the drag force at point D is higher than point C but slightly lower than point B. Similarly, although the velocity of the debris flow at the pipe location decreases with time, the intact and failed soil blocks hit the pipe by turns and therefore, a repetitive increase and decrease in the drag force become evident (Figure 7). Although this is a preliminary analysis and further investigations are needed, Figure 7 shows that the peak drag force on the pipe does not occur once rather depending on the progressive failure of the slope, pipe can experience the peak drag force or closer to the peak drag force more than once during the course of earthquake induced slope failure. Therefore, the progressive failure in sensitive clay plays an important role in the drag force. Similar F_D vs time graphs to Figure 7 are plotted for different parameters and discussed in the following sections.

5.3 Effect of change in s_{uR}

Figure 9 shows the effect of the change in remoulded shear strength, s_{UR} (= s_{u0}/S_t; where, S_t represents the sensitivity of the soil) on the drag force during the earthquake ($\leq$ 20s) and post–earthquake simulation (from 20-40s). The pipe (D = 300 mm) is placed at a distance, l = 10 m from the toe of the slope. Analyses are conducted for S_t = 1.5, 3.5 and 9. The drag force mobilizes differently with different s_{UR} (Figure 9). For a lower s_{UR}, the soil blocks displace at a higher velocity and therefore, the time to reach the peak drag force decreases with the decrease in remoulded shear strength (Figure 9).

5.4 Effect of the pipe location

To see the effect of the pipe location from the toe of the slope, three analyses are conducted with l = 10, 30 & 50 m for D = 300 mm. Figure 10 shows a trend of decreasing the peak F_D with l. For l = 10 m, the maximum, $F_{D(max)}$ = 175 kN/m (point B in Figure 10) whereas, for l = 50 m, $F_{D(max)}$ = 115 kN/m (point C in Figure 10). Such reduction in $F_{D(max)}$ is mainly due to the decrease of impact velocity and further reduction of s_u in l = 50 m case as compared to that of l = 10 m.

5.5 Effect of the pipe diameter

Figure 11 shows the effect of pipe diameter on the drag force. Analyses were conducted for two diameters D = 300 mm and 1000 mm for l = 10 m. Point B in Figure 11 shows the maximum drag force ($F_{D(max)}$ = 285 kN/m) calculated for D = 1000 mm is significantly higher than that of D = 300 mm (point C, Fig 11). However, $F_{D(max)}$ is not proportional to the diameter, which indicates that the typical normalization used for estimation of drag for non-sensitive clay (F_D/s_uD) may not be applicable in this case.

6 CONCLUSIONS

This study presents the preliminary simulation results of the effects of earthquake-induced sensitive clay landslides on an exposed section of a pipeline. The simulations are performed using a large deformation finite element modelling technique. The simulation results show that the maximum drag force is higher for a pipe closer to the toe.

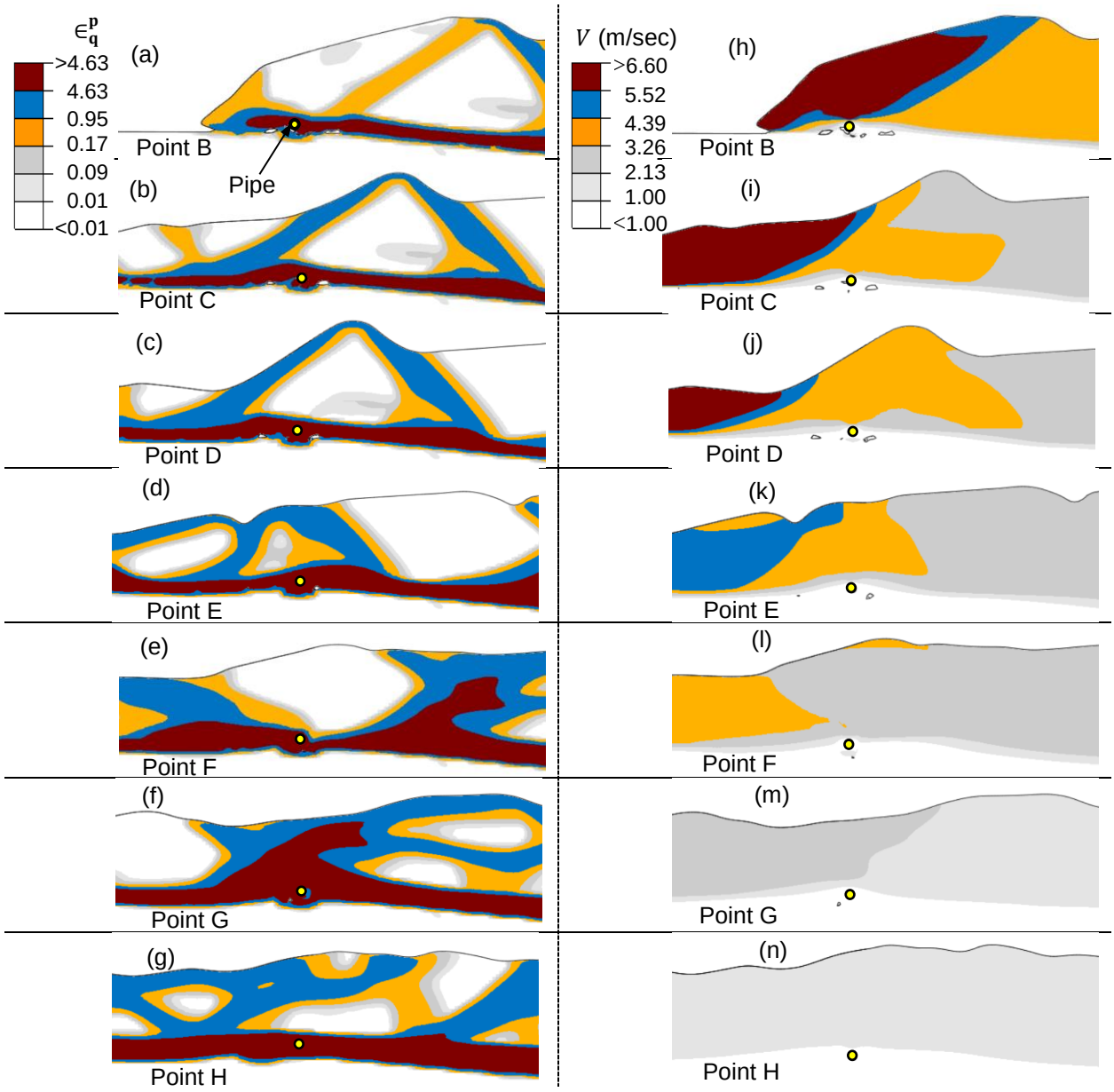

Figure 8. (a-g) Development of equivalent plastic strains and (h-n) instantaneous velocity during the earthquake and post-earthquake stage

The drag force does not increase monotonically to the peak value and remains constant, as commonly used to estimate the drag force resulted from debris flow—for example in offshore suspended pipeline. The mobilized undrained shear strength of the intact soil and highly remoulded soil along the failure planes of the soil block, together with downslope movement velocity, result in oscillation of the force with time. The analyses presented in this paper is only for idealized conditions.

7 ACKNOWLEDGMENTS

The authors express their sincere thanks to Dr. Rajib Dey, Dr. Sujan Dutta, Mr. Chen Wang and Mr. Diponkar Saha for their help with FE analysis and Northern Crescent Inc. for supporting the research project.

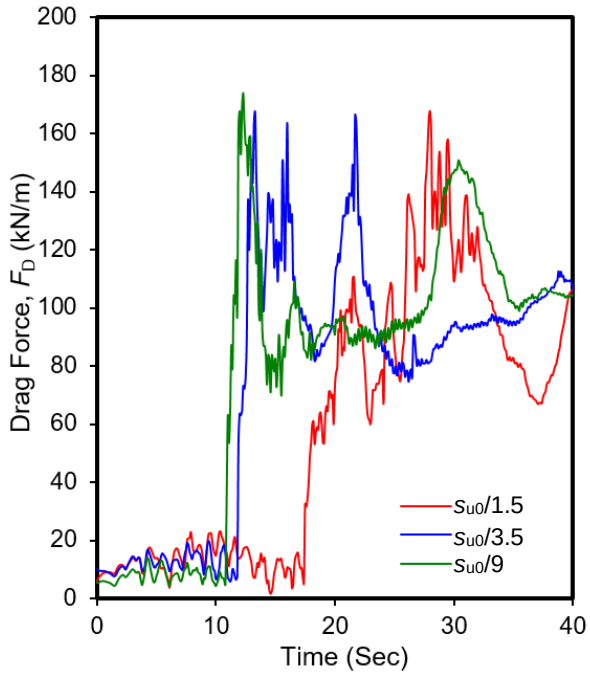

Figure 9. Effect of remoulded undrained shear strength

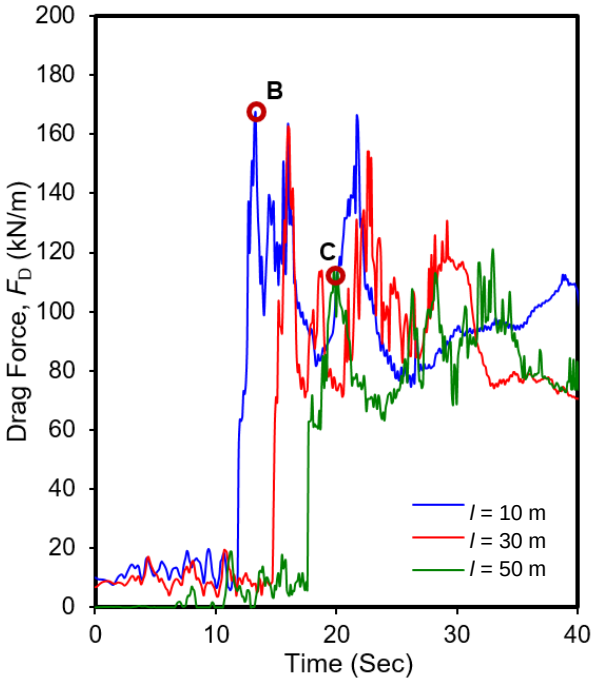

Figure 10. Effect of pipe location from the toe of the slope.

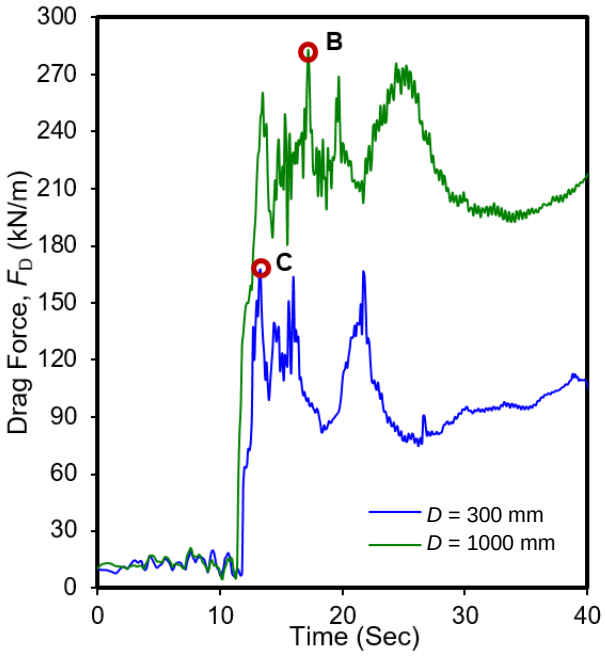

Figure 11. Effect of pipe diameter

REFERENCES

ABAQUS 6.14.2. D. S. Simulia, Dassault Systémes.

Choo, Y.W., Abdoun, T.H., O'Rourke, M.J. and Ha, D. 2007. Remediation for buried pipeline systems under permanent ground deformation. *Soil Dynamics and Earthquake Engineering*, 27(12):1043-1055.

Crofts, J.E., Menzies, B.K. and Tarzi, A.I. 1977. Lateral displacement of shallow buried pipelines due to adjacent deep trench excavations. *Géotechnique*, 27(2):161-179

Demers, D., Robitaille, D., Locat, P., and Potvin, J. 2014. Inventory of large landslides in sensitive clay in the province of Quebec, Canada: preliminary analysis. *In Landslides in Sensitive Clays: from Geosciences to Risk Management, Advances in Natural and Technological Hazards Research. Vol. 36. Edited by J.S. L'Heureux, A. Locat, S. Leroueil, D. Demers, and J. Locat. Springer*, Dordrecht, the Netherlands,77–89.

Desjardins, R. 1980. Tremblements de terre et glissements de terrain: Corrélation entre des datations au 14C et des données historiques à Shawinigan, Québec. *Géographie physique et Quaternaire*, 34(3):359-362.

Dey, R., Hawlader, B., Phillips, R., and Soga, K. 2015. Large deformation finite element modeling of progressive failure leading to spread in sensitive clay slopes. *Géotechnique*, 65(8): 657–668.

Dutta, S., Hawlader, B. and Phillips, R. 2015. Finite element modeling of partially embedded pipelines in clay seabed using Coupled Eulerian–Lagrangian method. *Canadian Geotechnical Journal*, 52(1):58–72

Eichhorn, G.N. and Haigh, S.K. 2018, September. Landslide Pipe-Soil Interaction: State of the Practice. *In 2018 12th IPC (pp. V002T06A014-V002T06A014). American Society of Mechanical Engineers.*

Einav, I., and Randolph, M.F. 2005. Combining upper bound and strain path methods for evaluating penetration resistance. *International Journal for Numerical Methods in Engineering*, 63(14): 1991–2016.

Filion, L., Quinty, F., and Begin, C. 1991. A chronology of landslide activity in the valley of Rivière du Gouffre, Charlevoix, Québec. *Canadian Journal of Earth Sciences*,28:250-256.

Girgin, S. and Krausmann, E. 2015. Lessons learned from oil pipeline natech accidents and recommendations for natech scenario development. *JRC Science and Policy Report*, EUR, 26913.

Islam, N., Hawlader, B., Wang, C. and Soga, K. 2018a. Large Deformation Finite Element Modeling for Earthquake-Induced Landslides Considering Strain-Softening Behavior of Sensitive Clay. *Canadian Geotechnical Journal*, https://doi.org/10.1139/cgj-2018-0250

Islam, N., Hawlader, B., Wang, C., and Soga, K. 2018b. Implementation of a large deformation finite element modeling technique for seismic slope stability analyses. *Soil Dynamics and Earthquake Engineering* (2nd review)

Klar, A. and Marshall, A.M. 2015. Linear elastic tunnel pipeline interaction: the existence and consequence of volume loss equality. *Géotechnique*, 65(9):788-792.

Lefebvre, G., Leboeuf, D., Hornych, P. and Tanguay, L. 1992. Slope failures associated with the 1988 Saguenay earthquake, Quebec, Canada. *Canadian Geotechnical Journal*, 29(1):117-130.

Leroueil, S. 2001. Natural slopes and cuts: movement and failure mechanisms. *Géotechnique*, 51(3): 197–243.

Masson, D.G., Harbitz, C.B., Wynn, R.B., Pedersen, G. and Løvholt, F. 2006. Submarine landslides: processes, triggers and hazard prediction. *Philosophical Transactions of the Royal Society A: Mathematical, Physical and Engineering Sciences*, 364(1845): 2009-2039.

Nadim, F. 1998. Slope stability under earthquake loading. Appendix F in Seabead project. NGI Report 982512-2.

Nyman, D.J., Lee, E.M., Audibert, J.M. and Geo-Technics, Q. 2008. Mitigating geohazards for international pipeline projects: Challenges and lessons learned. *Proc of the IPC.*

PEER. 2010. Ground motion database. Pacific Earthquake Engineering Research Center.

Pestana, J.M., and Nadim, F. 2000. Nonlinear site response analysis of submerged slopes. Report No. UCB/GT/2000-04. University of California, Berkeley,

Pike, K., Kenny, S. and Hawlader, B. 2014. Numerical and constitutive model development to aid design against pipeline geohazards. *Journal of Pipeline Engineering*, 13(1):201–209

Randolph, M. F. and White, D. J. 2012. Interaction forces between pipelines and submarine slides – a geotechnical viewpoint. *Ocean Engineering* 48: 32–37

Rathje, E. M. 2011. Geohazards Issues for the Enbridge Northern Gateway Project.

Roy, K., Hawlader, B., Kenny, S. and Moore, I. 2016. Finite element modeling of lateral pipeline-soil interactions in dense sand. *Canadian Geotechnical Journal*, 53(3): 490–504

Rumsey, P.B., Cooper, I. and Kyrou, K. 1982. Ground movement and pipe strain associated with trench excavation. In Restoration of sewerage systems (pp. 105-115). Thomas Telford Publishing.

Schwab, J.W., Geertsema, M. and Blais-Stevens, A. 2004. The Khyex River landslide of November 28, 2003, Prince Rupert BC Canada. *Landslides*, 1(3):243-246.

Stark, T.D., and Contreras, I.A. 1998. Fourth Avenue landslide during 1964 Alaskan earthquake. *Journal of Geotechnical and Geoenvironmental Engineering*, 124(2): 99–109.

Symons, I.F., Chard, B. and Carder, D.R. 1982. Ground movements caused by deep trench construction. *In Restoration of Sewerage System*. ICE publications, Thomas Telford, London, UK, 87–104

Tavenas, F., Flon, P., Leroueil, S., and Lebuis, J. 1983. Remolding energy and risk of slide retrogression in sensitive clays. *In Proc of the Symp on Slopes on Soft Clays*, Linkoping, Sweden, SGI Report No. 17: 423–454.

Tavenas, F. 1984. Landslides in Canadian sensitive clays–a state-of-the-art. *In Proc of the 4th International Symposium on Landslides*, Toronto, Ont (pp.16-21).

Trapper, P.A., Puzrin, A.M. and Germanovich, L.N. 2015. Effects of shear band propagation on early waves generated by initial breakoff of tsunamigenic landslides*. Marine Geology*, 370:99-112.

Wetmiller, R.J., Horner, R.B., Hasegawa, H.S., North, R.G., Lamontagne, M., Weichert, D.H., and Evans, S.G. 1988. An analysis of the 1985 Nahanni earthquakes. *Bulletin of the Seismological Society of America*, 78(2): 590–616.

Wijewickreme, D., Karimian, H. and Honegger, D. 2009. Response of buried steel pipelines subjected to relative axial soil movement. *Canadian Geotechnical Journal*, 46(7): 735-752.

Zakeri, A. 2009. Submarine debris flow impact on suspended (free-span) pipelines: Normal and longitudinal drag forces. *Ocean Engineering*, 36 (6): 489–499

Zakeri, A. and Hawlader, B. 2013. Drag forces caused by submarine glide block or out-runner block impact on suspended (free-span) pipelines - numerical analysis. *Ocean Engineering*, 67: 89–99